UC Irvine
UC Irvine Previously Published Works

Title
Electronic band structure and Kondo coupling in YbRh2Si2

Permalink
https://escholarship.org/uc/item/7595h83g

Journal
Physical Review B, 76(3)

ISSN
2469-9950

Authors
Wigger, GA
Baumberger, F
Shen, Z-X
et al.

Publication Date
2007-07-15

DOI
10.1103/physrevb.76.035106

Copyright Information
This work is made available under the terms of a Creative Commons Attribution License, availalbe at https://creativecommons.org/licenses/by/4.0/

Peer reviewed

eScholarship.org Powered by the California Digital Library
University of California

Electronic band structure and Kondo coupling in $YbRh_2Si_2$

G. A. Wigger, F. Baumberger, and Z.-X. Shen
Department of Applied Physics and Stanford Synchrotron Radiation Laboratory, Stanford University, Stanford, California 94305, USA

Z. P. Yin, W. E. Pickett, S. Maquilon, and Z. Fisk
Department of Physics, University of California, Davis, California 95616, USA

(Received 4 November 2006; revised manuscript received 22 March 2007; published 9 July 2007)

The electronic band structure of $YbRh_2Si_2$ is calculated in a relativistic framework including correlation corrections and magnetization of the Yb ion and compared to detailed angle-resolved photoemission spectra. The photoemission spectra for $LuRh_2Si_2$ are used as reference to identify electronic bands with no f symmetry. The calculated band structure manifests a $4f^{13}$ spin-polarized configuration leaving the unoccupied state at 1.4 eV above the Fermi energy. At the band theory level, the $4f$ bands are located far below the Fermi level and the anisotropic Coulomb interaction within the $4f$ shell spreads the multilevel into broader $4f$ complexes below −2.5 eV. The photoemission spectra obtained on $YbRh_2Si_2$ show a clear f-multilevel splitting into $j=7/2$ and $5/2$ excitations. The interaction of the $4f_{7/2}$ levels close to the Fermi energy with two conduction bands shows visible hybridization gaps of 45 and 80 meV, respectively. We discuss the origin of these excitations and provide an analysis according to Anderson's single-impurity model with parameters suggested by the band-structure calculation and the photoemission spectra. Both experiment and theory indicate nearly identical Fermi surfaces for $LuRh_2Si_2$ and $YbRh_2Si_2$. The valency of Yb in $YbRh_2Si_2$ is estimated to be close to +3.

DOI: 10.1103/PhysRevB.76.035106 PACS number(s): 71.27.+a, 79.60.−i, 71.15.Mb

I. INTRODUCTION

Heavy fermion (HF) systems on the border of a zero-temperature magnetic transition have been particularly attractive in the past years[1] because of their anomalous low-temperature thermodynamic, transport, and magnetic properties that deviate strongly from Landau Fermi liquid theory. Recently, an increasing number of examples of Ce- and U-based systems such as $CeCu_{6-x}Au_x$, $CePd_2Si_2$, $CeIn_3$, and U_2Pt_2In have been found to exhibit magnetic quantum criticality by either doping or pressure tuning.[2–5] $YbRh_2Si_2$ has attracted attention as the first observed Yb-based and stoichiometric HF system with competing Kondo and Ruderman-Kittel-Kasuya-Yosida interaction, i.e., the dominant exchange mechanisms in metals where the moments interact through the intermediary conduction electrons.[6,7] Indeed, in $YbRh_2Si_2$, a very weak antiferromagnetic order with a tiny magnetic moment of $\mu_{Yb} \approx (10^{-2}-10^{-3})\mu_B$ (Ref. 8) is observed at ambient pressure below the Néel temperature $T_N \simeq 70$ mK. Pronounced non-Fermi liquid behavior has been observed in the resistivity $\rho(T)$ and the electronic specific heat $\Delta C(T)$ at low temperatures, showing $\Delta\rho = \rho - \rho_0 \propto T$ and $\Delta C/T \propto -\ln(T)$, respectively.[9,10] The ground-state properties of $YbRh_2Si_2$ can be easily tuned around the magnetic quantum critical point by control parameters such as pressure, magnetic field, or doping.[1] An external pressure compresses the atomic lattice leading to an increase of the antiferromagnetic coupling with a maximal Néel temperature of 1 K at 2.7 GPa.[9,11] On the other hand, expanding the lattice by replacing Si by Ge (Ref. 12) or Yb by La favors the Kondo coupling and reduces T_N. Approximately 5% Ge or La doping completely destroys the antiferromagnetic order in $YbRh_2Si_2$. Electron-spin-resonance and nuclear-magnetic-resonance experiments have demonstrated the importance of magnetic fluctuations at low T.[8,13] At intermediate temperatures, a regime emerges for which it is believed that the quantum critical fluctuations dominate and the notion of a well defined quasiparticle breaks down. Remarkably, in $YbRh_2Si_2$, this regime extends up to 10 K.[10]

A Hall-effect measurement suggested a discontinuity in the Fermi-surface (FS) volume of one charge carrier across the quantum phase transition.[14] Based on a local-density approximation (LDA) calculation, the change in the FS volume by unit charge was suggested to arise from a shift of the f levels across a quantum transition from the antiferromagnetic phase to the Kondo Fermi liquid.[15] Concurring theories on critical heavy Fermi liquids assume f electrons to be partly integrated into a large FS and distinguish between visible quasiparticle peaks (spin-density wave case) versus a vanishing Kondo resonance.[16] A direct measurement of the electronic band structure and especially the location and renormalization of f-derived electronic bands, their hybridization with the conduction bands, and their incorporation into the FS could provide a stringent test of such theories. Angle-resolved photoemission spectroscopy (ARPES) has proven to be uniquely powerful in its capability to directly probe the electronic structure of solids.[17]

We report here the band-structure calculations reflecting the Yb^{3+} ion that is observed by macroscopic experiments at elevated temperatures. Previous calculations have only modeled a nonmagnetic Yb^{2+} ion. We compare the angle-resolved photoemission spectra for $YbRh_2Si_2$ in the ordinary Kondo-screened state with those for $LuRh_2Si_2$. The comparison of the Yb and Lu compounds provides a definitive identification of the $4f$-derived states in the Yb compound. Most importantly, we have directly observed evidence of hybridization between the $4f$ state and valence states, yielding hybridization gaps ranging from 30 to 80 meV. We performed an analysis of the $4f$-derived spectrum $\rho_\nu(\epsilon)$ within the single-impurity Anderson model[18] using parameters sug-

 ©2007 The American Physical Society

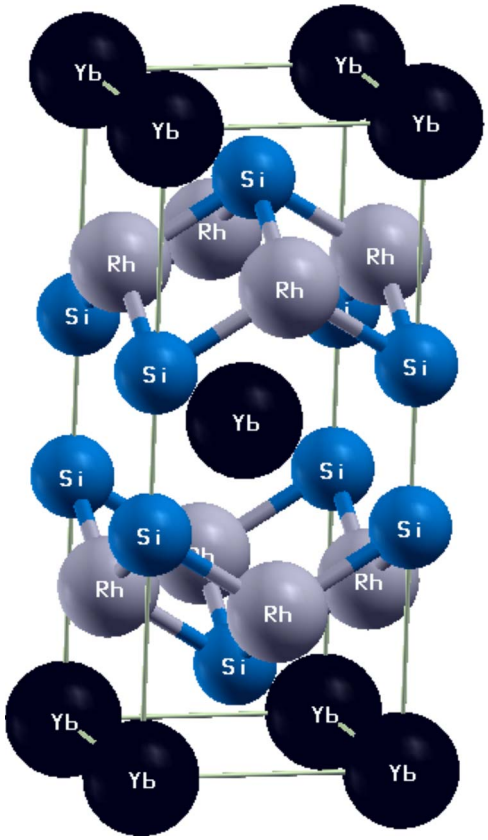

FIG. 1. (Color online) Crystal structure of $YbRh_2Si_2$.

gested by the band-structure calculation, which leads to a picture that differs from those presented in previous studies. This analysis explains $\rho_\nu(\epsilon)$ and macroscopic parameters such as the Kondo temperature T_K in reasonable agreement with the experiments.

II. ELECTRONIC STRUCTURE CALCULATIONS

A. Structure

The crystal structure of $YbRh_2Si_2$, displayed in Fig. 1, is body-centered tetragonal (bct) with $I4/mmm$ space group (space group 139). The Yb ion occupies the $2a$ site which has full tetragonal $4/mmm$ symmetry and forms a bct sublattice, which becomes important in the interpretation of its magnetic behavior. Rh resides in a $4d$ site ($\bar{4}m2$ symmetry) and lie on a simple tetragonal sublattice rotated by 45° in the plane and having lattice constants $a/\sqrt{2}$ and $c/2$. Si is in the $4e$ site ($4mm$); the Si-Si interatomic distances of 2.46 Å is only 5% longer than in diamond structure Si, so one view of the structure is in terms of Si_2 dimers oriented along the $\hat{z}$ axis. Yb atoms and the dimers form a centered square lattice in the x-y plane. Yb is eightfold coordinated by Rh at a distance of 3.17 Å. The atomic positions are [in units of (a,a,c)] Yb (0,0,0), Rh $\left(0,\frac{1}{2},\frac{1}{4}\right)$, and Si (0,0,0.375); note that the Si height is not determined by symmetry and is accidentally equal to $\frac{3}{8}$. The experimental lattice constants $a=4.010$ Å and $c=9.841$ Å have been used in our calculations.

For reference, we have also calculated the band structure of isostructural and isovalent $LuRh_2Si_2$ ($a=4.090$ Å, $c=10.18$ Å). In this compound, Lu has a filled $4f$ shell under all conditions and the compound is a conventional nonmagnetic metallic Fermi liquid.

B. Methods

Rare-earth atoms and other atoms with strong effective intra-atomic Coulomb repulsion U (Hubbard U) pose a serious challenge for band theoretical methods. Density-functional theory addresses at the most basic level the ground state, which gives the Hund's rule ground state of the Yb ion a central role. Hund's rule implies that one leaves consideration of spin-orbit coupling (SOC) until after the spin S and angular momentum L have been maximized. On the other hand, for interpreting single-particle-like excitations, which is the main topic of this paper, one wants to obtain the $j=\ell\pm\frac{1}{2}$ character of the excitations. Thus, one must include SOC at the one-electron level, and that is the viewpoint that we take here. From the Curie-Weiss susceptibility at high temperature in $YbRh_2Si_2$, it is clear that the Yb ion is primarily in a $4f^{13}$ configuration (at elevated temperature, at least), corresponding to $S=\frac{1}{2}$, $L=3$, and $J=\frac{7}{2}$ in the absence of crystal fields.

To be able to include the necessary combination of exchange splitting (magnetic order), SOC, and also the local-density approximation plus intra-atomic repulsion U (LDA $+U$) approach that is necessary for rare-earth atoms, we have used the WIEN2K electronic structure code.[19] An f^{13} configuration necessarily requires a magnetic ion, and we consider only the simplest (ferromagnetic) alignment of Yb spins. With magnetization along the (001) direction, SOC reduces the symmetry to $Abm2$ (space group 39). The around-mean-field version of LDA$+U$ (appropriate for small spin) was used, with $U=8$ eV and $J=1$ eV. In the results presented below, the $m=0$ $4f$ orbital was unoccupied. We have also obtained a solution with the $m=-2$ orbital unoccupied. (The Hund's rule state would have $m=+3$ unoccupied.) There is no difference in the results that are discussed here, only minor differences in the placement of the Yb $4f$ bands. The filled f^{14} shell of Lu does not present any of these complications. To obtain an accurate determination of the Fermi surface, we have used a k mesh of 20^3 (641 k points in the IBZ), $R\,K_{max}=9$, and the Perdew-Burke-Ernzerhof generalized gradient approximation[20] for exchange-correlation potential. An energy range from −7 to 7 Ry is used when SOC is incorporated.

C. Band-structure results

The band structure of $YbRh_2Si_2$ shown in Fig. 2 is characterized by the expected $4f^{13}$ spin-polarized configuration of the Yb ion. Without SOC, this would correspond to one hole in the minority $4f$ shell. With SOC included, as here, the flat $4f$ band complex is spin mixed and split into a $4f_{5/2}$ complex and a $4f_{7/2}$ complex separated by the spin-orbit splitting of roughly 1.3 eV. Although each $4f$ band is quite flat, each of the complexes of $2j+1$ bands $\left(j=\frac{5}{2},\frac{7}{2}\right)$ is split

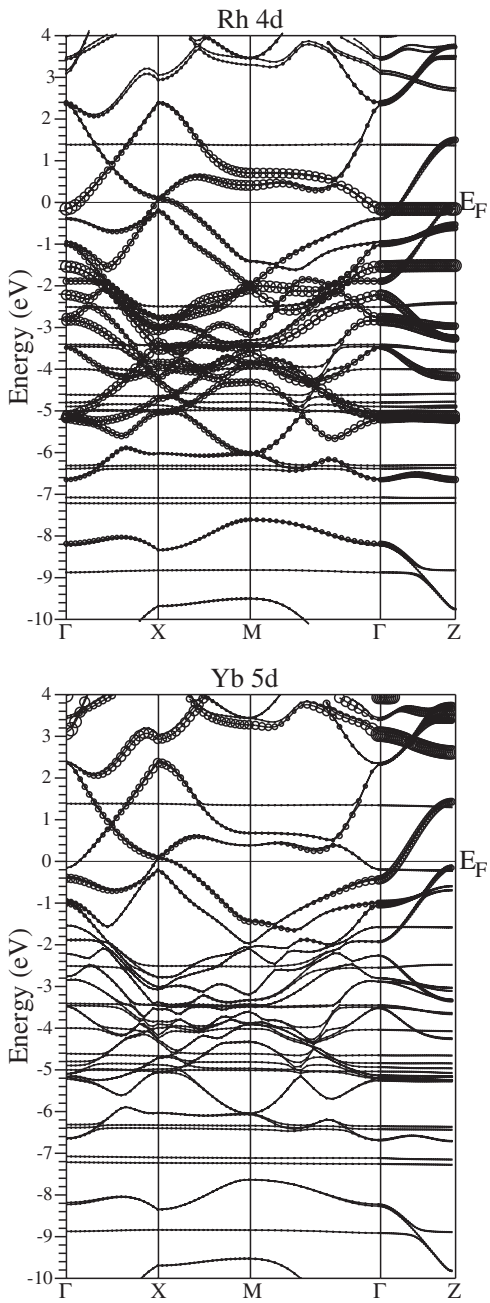

FIG. 2. Band structure of $YbRh_2Si_2$ along tetragonal symmetry lines. The Cartesian symmetry line indices are $\Gamma(0,0,0)$, $X(1,0,0)$, $M(1,1,0)$, and $Z(0,0,1)$ in units of $\left[\frac{\pi}{a},\frac{\pi}{a},\frac{2\pi}{c}\right]$. Top panel: bands with total Rh $4d$ emphasized using the flatband representation. Bottom panel: same bands with total Yb $5d$ emphasized using the flatband representation.

due to the anisotropy of the Coulomb interaction[21] within the $4f$ shell, which is included fully in the LDA+U method. However, the $4f$ electrons are polarized (one hole, $S=\frac{1}{2}$), which also induces a Hund's (exchange) splitting that complicates the identification in the figure of the $4f_{5/2}$ and $4f_{7/2}$ states separately. However, the result that is pertinent to this paper is that this electronic structure calculation fully includes magnetic and relativistic effects and intra-atomic correlation in a static but self-consistent manner and leaves one

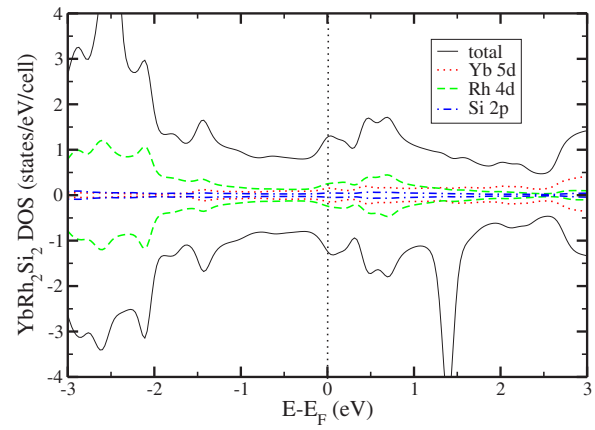

FIG. 3. (Color online) Total and projected (per atom) densities of states of $YbRh_2Si_2$ corresponding to the band structure in Fig. 2. Rh $4d$ character dominates around the Fermi level.

hole in the $4f$ shell consistent with the Curie-Weiss susceptibility.

The unoccupied $4f$ band lies 1.4 eV above the Fermi level E_F and can be seen to mix exceedingly weakly with the itinerant (Rh+Yb+Si) bands, reflecting its very localized character. The occupied levels lie 2.5 eV or more below E_F and also hybridize weakly. Hence, at the band-structure level, the $4f$ states are well away from the Fermi level. Many-body interactions arising through coupling to the conduction bands may, of course, lead to large renormalizations as reflected in the experimental data (see Sec. I). We focus first on the states near and at E_F, and then return to the (Kondo) coupling of the $4f$ moment to the Fermi surfaces.

The total Rh $4d$ and total Tb $5d$ characters are shown separately in the projected orbital character representations in Fig. 2. (See Fig. 3 for the density of states.) Much of the Rh $4d$ bands are occupied, while most of the Yb $5d$ bands are unoccupied; however, there is Yb $5d$ character around and even below the Fermi level. The Si $3p$ character is spread fairly evenly through the valence and conduction bands. The bands around E_F have mostly Rh $4d$ character, with some Yb $5d$ mixed in, and the bands along symmetry lines are clearly associated with certain symmetry-determined irreducible representations $a_g(d_{3z^2-r^2})$, $b_{1g}(d_{x^2-y^2})$, $b_{2g}(d_{xy})$, or $e_g(d_{xz},d_{yz})$ of the Rh and Yb d states.

The first noteworthy feature is the band lying 0.2 eV below E_F at Γ, which is completely flat along Γ-Z [$(0,0,k_z)$ line] and disperses upward in the plane: this is a pure Rh $d_{x^2-y^2}$ band. There is also a strong Rh $4d_{x^2-y^2}$ character at -5 eV (within the $4f$ bands), presumably the bonding combination of $d_{x^2-y^2}$ orbitals on the two Rh atoms in the cell. The Rh $d_{x^2-y^2}$ band crossing E_F contributes the cylindrical faces of the electron-type tall pillbox $\mathcal{P}$ FS with (near circular) mean radius in the plane of $k_F=0.133\frac{\pi}{a}$. All three FSs are displayed in Fig. 4. The Fermi level is intersected along Γ-Z by a band composed of Rh $4d_{3z^2-r^2}$, Yb $5d_{3z^2-r^2}$ character and 2 eV wide. This band defines the top and bottom faces of the Γ-centered pillbox, with Fermi wave vector $k_F=0.265\frac{2\pi}{c}$ along the $\hat{z}$ axis. This pillbox contains $\sim 4\times 10^{-3}$ carriers/f.u.

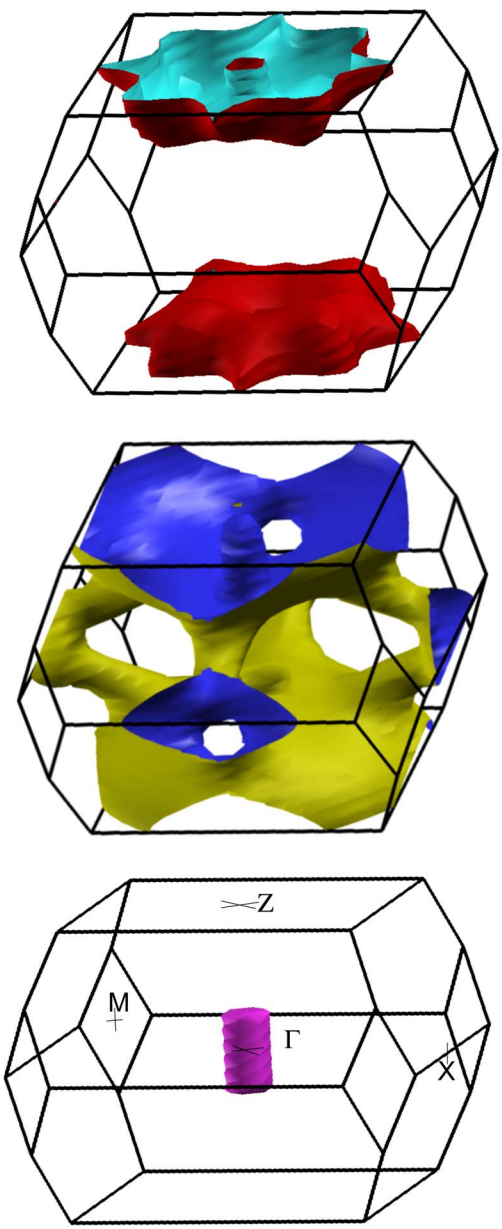

FIG. 4. (Color online) The three calculated Fermi surfaces of $YbRh_2Si_2$ with $4f^{13}$ configuration, pictured within the crystallographic Brillouin zone. Top panel: fluted donut $\mathcal{D}$ surface centered around the upper zone face midpoint Z. Middle panel: multiply connected jungle-gym $\mathcal{J}$ surface. Bottom panel: tall pillbox surface $\mathcal{P}$, containing electrons at the zone center Γ. The Fermi surfaces of $LuRh_2Si_2$ are very similar; see text.

From the bands in Fig. 2, it can be observed that a hole-type surface nearly closes at the $X=\left(\frac{\pi}{a},0,0\right)$ point. Because the point we call X is not on the bct Brillouin-zone boundary (the true zone is shown in Fig. 4), this is not a small ellipsoid as might be guessed, but rather part of tubes of a multiply connected jungle-gym surface $\mathcal{J}$. The largest part of this surface encircles nearly all of the upper zone face centered on the $Z=\left(0,0,\frac{2\pi}{c}\right)$ point. The character near X is Rh $4d_{xz}$, $4d_{yz}$ and some Yb $5d$ character. There is also strong Rh $4d_{xz}$, $4d_{yz}$ character in the flatband along Γ-Z near -3 eV. Rh $4d_{xy}$ character dominates the flatband at -1.5 eV along Γ-Z, which disperses downward from there within the plane.

The other Fermi surface, also shown in Fig. 4, is a fluted donut $\mathcal{D}$ centered at the Z point and oriented in the x-y plane. It arises partially from the upward dispersion in the x-y plane of the band that lies at -30 meV at Z. This donut $\mathcal{D}$ surface contains electrons.

The FS of $LuRh_2Si_2$ is nearly identical, as anticipated from the identical structures and the isovalence of the rare-earth ions. One change occurs due to a small difference in band energy at and near the X point. The $\mathcal{J}$ surface changes its connectivity and shape as a result but remains a large (and generally similar) FS.

D. Aspects of Kondo coupling

$YbRh_2Si_2$ is a heavy fermion compound, whose $J=L+S=\frac{7}{2}$ ion and associated local moment will be affected by crystal fields and finally screened by conduction electrons at low temperature (a tiny moment survives and orders in $YbRh_2Si_2$; see Sec. I). Thus, while our ferromagnetic state with $S=\frac{1}{2}$ is not expected to describe the interacting ground state, it has the virtue of providing a measure of the degree of Kondo coupling of the Yb moment to the Fermi surfaces, because the exchange splitting of the Fermi surfaces reflects the coupling of the local moment to the itinerant bands.

The exchange splitting of the Γ cylinder is 6 meV around its waist (in the x-y plane) and 30 meV at top and bottom, a strong anisotropy resulting from the different characters of wave functions on the different parts of the surface. For points on the $\mathcal{J}$ surface near the X point, the exchange splitting is 20 meV at both $(0.95,0,0)\frac{\pi}{a}$ and $(1,0.2,0)\frac{\pi}{a}$. Thus, the Kondo coupling, and likewise the carrier scattering by the moments, differs by at least a factor of 5 around the Fermi surfaces.

E. Discussion of bands and Fermi surfaces

This fully relativistic, spin-polarized LDA+U band structure and resulting Fermi surfaces can be compared with previous unpolarized relativistic LDA prediction.[15,22,23] Not surprisingly, there are substantial differences, as expected from the LDA's $4f^{14}$ configuration versus our magnetic $4f^{13}$ bands; this difference in Yb $4f$ charge state puts Norman's Fermi level one electron lower with respect to the Rh $4d$ +Yb $5d$+Si $3p$ itinerant bands.[15] As a result, the flat Rh $4d_{x^2-y^2}$ band that lies 0.2 eV below E_F in our bands lies 0.1 eV *above* E_F in the LDA bands, and the Fermi surfaces are entirely different. These differences will lead to completely different predictions for the Hall coefficient.

On the qualitative level, our Fermi surfaces include large sheets with canceling positive and negative contributions to the Hall coefficient, as do Norman's. The Hall coefficient, usually thought of (in the constant relaxation times approximation) as being an average of the Fermi-surface curvature, will bear no relation to the number of carriers. No doubt it will be quite anisotropic, given the strong tetragonality of the FSs. The edges of the pillbox $\mathcal{P}$ may give large contributions (and make evaluation difficult); likewise, the sharp edges on the donut $\mathcal{D}$ will also have large curvatures.

The "curvature" interpretation of the Hall tensor relies on the isotropic scattering time approximation. This situation is unlikely to be the case in $YbRh_2Si_2$, where the main scattering arises from the Kondo coupling to local moments. As pointed out in the previous section, this coupling varies strongly over the Fermi surface (by at least a factor of 5). Hence, this system is an example of a multiband (correlated) metal with large Fermi surfaces of varying curvature, having large and anisotropic scattering. Its Hall tensor, versus temperature, field, and magnetic ordering, promises to be very challenging to understand.

III. EXPERIMENTS

Millimeter sized single crystalline platelets of $LuRh_2Si_2$ and $YbRh_2Si_2$ were grown by the flux-growth method using an In flux in a sealed Ta tube under argon atmosphere. The crystals were washed in HCl acid solution to safely remove excess In flux. The tetragonal crystal structure and the lattice parameters were confirmed by x-ray powder diffraction.

The ARPES measurements were performed using a chamber equipped with a Scienta SES200 analyzer attached to the undulator beamline 5-4 of the Stanford Synchrotron Radiation Laboratory (SSRL) and a second vacuum system equipped with a Scienta SES2002 analyzer and a microwave driven monochromatized He-discharge lamp (Gammadata VUV5000). At SSRL, we used linearly polarized photons of 21.4 eV. The photoemission spectra at these photon energies allow a detailed comparison of the electronic states with no f symmetry in $LuRh_2Si_2$ and $YbRh_2Si_2$. We intentionally refrained from tuning the photon energy to resonance with Yb core levels, which enhances the photoelectron yield of the Yb $4f$ electrons but worsens the energy resolution by approximately six to eight times. At these low energies, the photoelectron mean free path becomes very short and care has to be taken regarding identifying surface and bulk states. Fortunately, there are numerous reports having dealt with this issue in Yb-related materials[24,26,27] and also in $YbRh_2Si_2$.[22] An energy resolution of $\sim$40 meV or more hides the relevant hybridization features in the angle-resolved spectra for the critical system $YbRh_2Si_2$. The total energy resolution including the monochromator and the analyzer was 8 meV for the 21.2 eV beam from the He source and 22 meV for the 21.4 eV synchrotron beam, respectively. The chamber pressure was below 4×10^{-11} torr. The samples were cleaved *in situ* at $T\sim14$ K. As opposed to previous experiments on Yb- or Ce-based material, very clean cleaves with large flat grayish shiny areas can be obtained on these 1-2-2 compounds where the electronic spectra manifest sharp features. The excellent quality of the surface has been determined using high-resolution low-energy electron diffraction. The position of the Fermi level (E_F) was calibrated from the Fermi edge of polycrystalline Au for every measurement.

IV. PHOTOEMISSION RESULTS AND DISCUSSION

A. Angle-integrated spectrum at $h\nu$=40.8 eV

Figure 5 shows the angle-integrated spectrum for $YbRh_2Si_2$ (solid curve) at angles between −5° and 17° in the

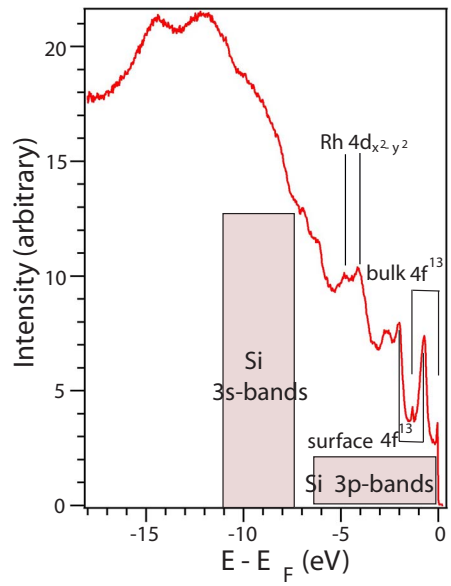

FIG. 5. (Color online) Angle-integrated PE spectrum (solid curve) of $YbRh_2Si_2$ measured with photon energy of 40.8 eV at 14 K. The lines are explained in Sec. IV A.

Γ-M-Z plane measured with He II radiation. The broad distribution of intensity between −11 and −7.5 eV, indicated by the shaded area in Fig. 5, included emission from Si $3s$ states, as indicated by the band-structure calculations. At low binding energies, we can identify two sharp but small intensity maxima at $\sim$−1.3 eV and right at E_F with a peak intensity ratio of approximately 2:3, respectively. The corresponding data for $h\nu$=21.2 eV do not display any pronounced intensity at these energies. Hence, these are single-hole, very weakly hybridized $j=7/2$ and $j=5/2$ states split by the 1.3 eV SOC energy (see Sec. IV C). The intense peaks at 650 meV and at 2 eV can be attributed to the spin-orbit split surface bands[28] originating from Yb ions at or close to the sample surface. The relative intensity of surface vs bulk peaks decreases strongly when the photon energy is increased from 21 to 41 eV and 110 eV.[22] The intensity around 3 eV is not due to flatbands but is a result of various coterminating band edges having high intensities in that energy region, which is seen in the angle-resolved spectrum in Fig. 7. We refer to Ref. 22 where the $4f$ intensities can be compared to the atomistic calculations of Gerken.[29] However, this paper focuses on the excitations close to the Fermi energy, related to the Yb $4f^{13}_{7/2}$ excitations.

B. Angle-resolved spectra for $LuRh_2Si_2$ and $YbRh_2Si_2$

Within the sudden approximation,[17] angle-resolved photoemission measures the single-particle spectral function $A(k,\omega)$, where k is the crystal momentum and ω is the photohole energy taken at a beam energy $h\nu$=21.2 eV. For quasi-two-dimensional materials, it is the in-plane component of the crystal momentum $k_\parallel$ that matters. We will plot the data with respect to $k_\parallel$; however, we note that the three-dimensional behavior can be important in this material. $\tilde{\Gamma}$, $\tilde{M}$, $\tilde{X}$, and $\tilde{Z}$ refer to locations in the Brillouin Zone (BZ)

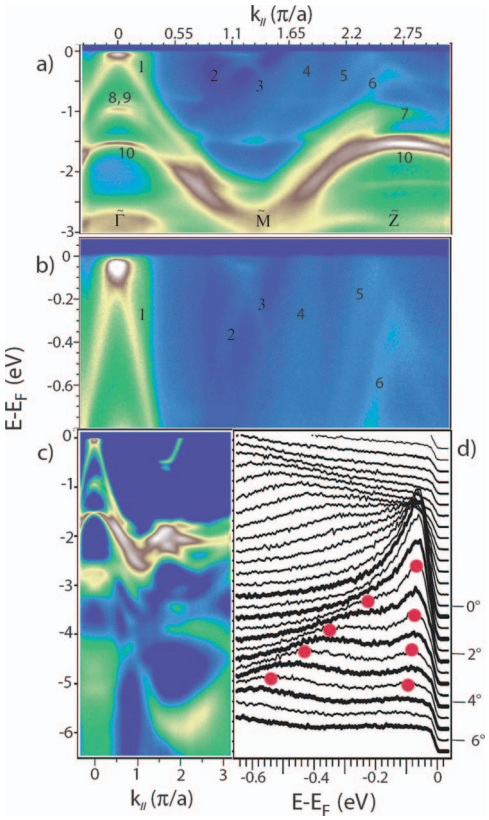

FIG. 6. (Color online) [(a) and (b)] Angle-resolved PE spectra for $LuRh_2Si_2$ taken in our case at 21.2 eV in the $\tilde{\Gamma}\tilde{M}$ direction. The numbers are referred to in the text. (c) Angle-resolved spectrum of $LuRh_2Si_2$ in the $\tilde{\Gamma}\tilde{X}$ direction. (d) EDC plot for the ΓM direction near $\tilde{\Gamma}$.

close to the Γ, M, X, and Z points in the real BZ, respectively. The three-dimensional nature of the bands, and hence of the photoemission process, inhibits more precise identification in k space (i.e., of k_z). The distance $\tilde{\Gamma}\tilde{X}$ is approximately equivalent to ΓX in the center of the BZ. In order to connect to the calculations, we use ω, ϵ, and $E-E_F$ on an equal basis in the following discussions.

At the most rudimentary level, $LuRh_2Si_2$ and $YbRh_2Si_2$ differ only by one electron in the $4f$ shell on the rare-earth ion. Whereas high-temperature experiments have shown that in these materials Yb is in the magnetic $4f^{13}$ state, Lu has a filled shell and the $4f$-electron levels are expected to be at elevated binding energies. Hence, comparing photoemission results for these compounds can yield insight into the nature of the various electronic bands with no f symmetry.

$LuRh_2Si_2$. The top two plots in Fig. 6 show the angle-resolved photoemission spectra for $LuRh_2Si_2$ in the $\tilde{\Gamma}$-M-Z-plane with different energy scales measured at 21.2 eV. Comparing the energy distribution curve (EDC) and the FS images to the results of the band-structure calculations, we conclude that $\tilde{\Gamma}$ lies on a point slightly below 1/4 of the line from $-Z$ to Γ. Several bands — 1, 2, 3, 4, and 5 — cross the Fermi level and form Fermi surfaces. Since the LDA calculation for $LuRh_2Si_2$ yields nearly the identical FS as the LDA+U+SOC calculation does for $YbRh_2Si_2$, these

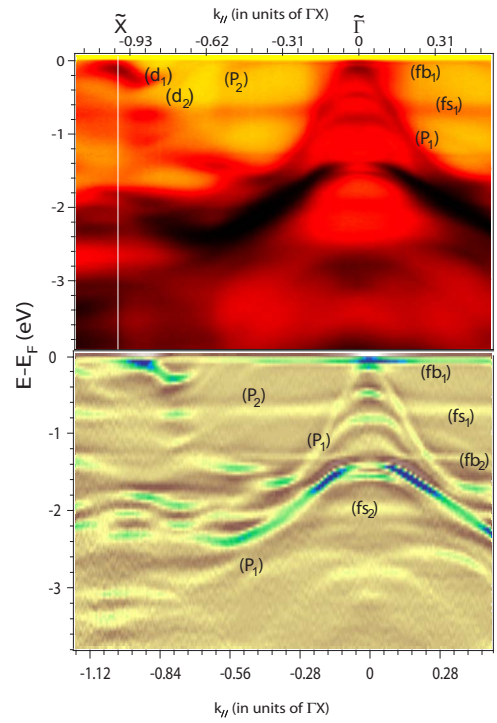

FIG. 7. (Color online) Angle-resolved PE spectra of $YbRh_2Si_2$ taken at $h\nu$=21.4 eV at T=14 K in the Γ-X-Z plane. The lower panel shows the second derivative of the spectrum (upper panel). The relevant bands are denoted as (fb_1) and (fb_2) for the bulk $4f^{13}$ and (fs_1) and (fs_2) for the surface $4f^{13}$ states; P_1 and P_2 are valence bands with mostly Rh $4d$ and partly Yb $5d$ character, for the latter one.

sheets can be compared to the corresponding ones in Fig. 4. Bands 4 and 5 are already in the neighboring BZ. They can be ascribed to the donut shaped $\mathcal{D}$ and jungle gym $\mathcal{J}$ FSs, respectively. Band 1, i.e., the Rh $4d$ band, shows a parabolic dispersion where the spectral weight increases strongly as E_F is approached near $\tilde{\Gamma}$. The lower right panel in Fig. 6 reveals, however, that it is not only a single band but also a steep one (band 1) and a flat one (band 1′) meeting at $\tilde{\Gamma}$ without opening a clearly detectable hybridization gap.

$YbRh_2Si_2$. The upper panel in Fig. 7 shows an angle-resolved photoemission spectrum in the Γ-X-Z plane measured again at the same 21.2 eV. Compared with the $LuRh_2Si_2$, we have evidence for four additional bands between E_F and 2 eV binding energy, suggesting that these are Yb-derived $4f$ states, an assignment consistent with these bands being extremely flat. Two different flatbands display a pronounced intensity: band (fb_1) located very close to E_F and band (fs_1) with a maximum intensity at ≈680 meV below E_F. The latter is derived from electronic states of Yb atoms close to the sample surface (see Sec. IV A). Previous spectroscopic experiments[30] and fully relativistic calculations (see Fig. 2) revealed that the spin-orbit interaction in Yb-based materials is of the order of 1.3 eV, consistent with the value obtained within the relativistic calculation (see Sec. II).

Masked in the primary spectra by the high intensity of neighboring bands, the second derivative plot (lower panel in

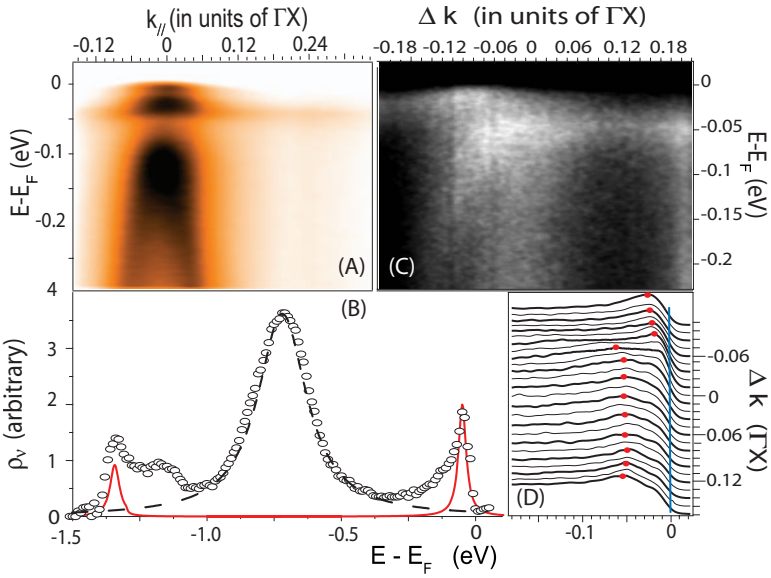

FIG. 8. (Color online) (A) Experimental PE spectrum for small energies in the vicinity of $\tilde{\Gamma}$. (B) The empty circles represent the spectrum solely due to the $4f$ final states obtained as explained in the text. The solid line is a calculation according the GS scheme explained in the text. The long-dashed line is a Lorentzian to the surface peak. The right panels show the hybridization of the f band with the band (P_2). Panels (C) and (D) show the spectrum where bands (P_2) and (fb_1) hybridize. The zero in the Δk axis denotes the wave vector $k_{\parallel}=0.385\Gamma X\cdot(0.985,0.174)$ and we measure along the yellow line in Fig. 9.

Fig. 7) reveals a third very flat electronic band (fb_2) separated from band (fb_1) by the spin-orbit splitting $\Delta\epsilon_f \approx 1.3$ eV and a fourth flatband (fs_2) 1.3 eV below band (fs_1), i.e., the bulk and surface $4f_{5/2}^{13}$ final states, respectively. Neither a careful investigation of the spectra nor the second derivative plot revealed an additional flatband with f symmetry as indicated by the LDA+U+SOC band-structure calculation. This observation reflects the fact that the LDA+U eigenvalues are not in one-to-one correspondence with photohole energies in open strongly correlated shells, and more especially so when there is important coupling to valence states as is clearly the case in $YbRh_2Si_2$. Hence, the f excitations are split into a $4f_{5/2}$ peak at ~ -1.3 eV and a sharp band of $4f$ electrons with $j=7/2$ centered at ~ -45 meV with a peak width of $\Gamma_{FWHM} \approx 30$ meV obtained from an EDC fit to a Lorentzian shape.

A strong intensity is displayed by the band (P_1) which shows a nearly-free-electron parabola with band width B down to -3.6 eV at the X point and nearly 6 eV at the M point (see lower left panel in Fig. 6). While the band consists of several overlapping components, comparison with LDA+U band structure suggests that it is mostly states of Rh $4d$ character. While the real band structure is more complicated, we will use a nearly free parabola to mimic this band for continuation $\epsilon > 0$ eV and simulating the $4f$ spectral weight later. Moreover, band (P_1) also crosses and mixes with the Yb-derived surface bands (fs_1) and (fs_2) around $\tilde{\Gamma}$. Since the Si ions form strongly bonded Si_2 dimers that encage the Yb ions, the first Yb layer is intermediate between a bulk and a surface layer such that it can be distorted by hybridization with a bulk band.

Halfway between the $\tilde{\Gamma}$ and the $\tilde{X}$ point, a band (P_2), displaying a very weak intensity, hybridizes with the f band. We will show in Fig. 8 how this hybridization arises. This band (P_2) starts at approximately -2 eV close to M and crosses E_F near X as observed in Fig. 2. Considering the wave-function symmetry of this band, it can be continued in a nearly free parabola to approximately 2 eV above E_F at Γ. This band induces the holelike FS $\mathcal{D}$. At $\sim 20°-25°$, we observe two different bands denoted as (d_1) and (d_2). They form the jungle-gym FS sheet $\mathcal{J}$ and will be briefly discussed in the Sec. IV D.

The upper left panel in Fig. 8 shows $A(k_{\parallel},\omega)$ measured in the vicinity of $\tilde{\Gamma}$ using a photon energy of 21.2 eV. At very small angles, the $4f_{7/2}$ band (fb_1) with peak width less than 35 meV hybridizes weakly with the Rh $4d$ band leading to a dispersion of ≈ 10 meV. A gap between the peaks of the two bands of approximately 80 meV is observed. For $\omega \geqslant -20$ meV, $A(k_{\parallel},\omega)$ rises again toward lower binding energies indicating a double peak structure. In analogy to the spectra for $LuRh_2Si_2$, we observe a similar double peak structure between two dispersing Rh bands, but now they are separated by an Yb f band. Nearly no dispersion is observed for the peak below 20 meV binding energy. We note here that this feature near E_F does not follow the dispersion behavior of the f band, but it is rather limited to a small region around $\tilde{\Gamma}$. Furthermore, as we change the photon energy between 17 and 31 eV, the intensity at E_F remains almost unchanged (not shown here), characteristic for a band with minimal dispersion in the k_z direction. Hence, this lowest-energy peak at Γ cannot be considered as a candidate for the Kondo resonance as it has a corresponding component in $LuRh_2Si_2$.

Panels (C) and (D) in Fig. 8 show a photoemission spectrum along the yellow line in Fig. 9. The top-right panel shows the raw data; the bottom right is the corresponding EDC data. The filled circles are obtained by fitting a single Lorentzian and a constant background to the EDC curves and the vertical thick line sets the Fermi level. A steep band [band (P_2) in Fig. 7] with strong Rh d character hybridizes with the flat Yb f band. This induces an opening of a band gap of the order of 30–40 meV. We note that this gap is too small to incorporate significant f spectral weight into the FS.

C. 4*f*-excitation spectrum

Now, we now come back to the $4f$ states. As in Ref. 22, there is a complex $4f$ spectral weight for binding energies above 4 eV, consistent with the LDA+U+SOC calculation

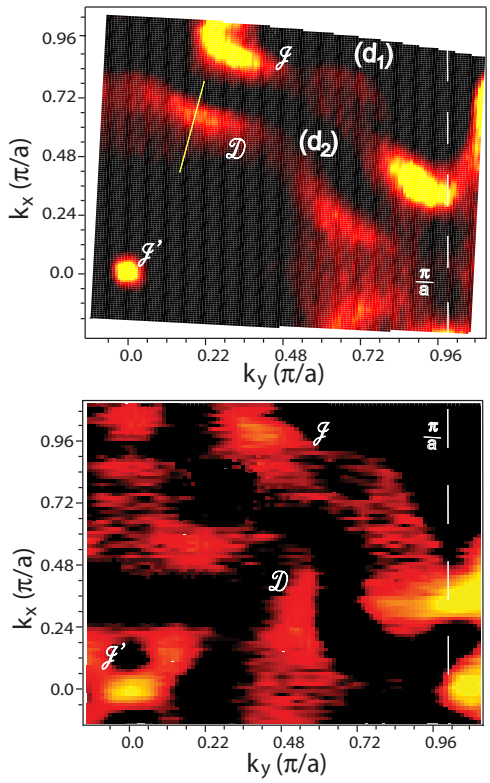

FIG. 9. (Color online) In the lower panel, we plotted a Fermi-surface map for $LuRh_2Si_2$ taken at 21.2 eV. The upper panel shows the corresponding map for $YbRh_2Si_2$. $\mathcal{J}'$, $\mathcal{D}$, and $\mathcal{J}$ are three different FS parts as discussed in the text. The dashed line indicates $\frac{\pi}{a}$, where a is the length of the lattice bases. Units are given in $\frac{\pi}{a}$.

in Fig. 2. Unlike band theory, we observe two $4f$-derived bulk features between E_F and −1.3 eV arising from many-body interactions. They are usually related to $4f_{7/2}$ and $4f_{5/2}$ excitations and denoted as the Kondo resonance and its spin-orbit side band.[24,25] The additional splitting due to an anisotropic Coulomb interaction that would lead to distinct energies of different $l=3$ hole orbitals is not observed.

We have performed a Gunnarsson-Schönhammer[25] (GS) analysis using parameters suggested by the band-structure calculations which differ significantly from those normally used in the literature.[24–26,31] This scheme employs a second-order perturbative calculation based on the Anderson single-impurity model. We will assume $U=\infty$ and a large SOC in order to study only the $4f_{7/2}^{13}$ states with degeneracy $N_f=8$.

As is usual in GS calculations, we model the valence band with a semielliptical density of states, in our case extending from −6 to 6 eV. Based on our earlier discussion, we represent the P_2 band with a half-filled semielliptical form ranging from −1.8 to 2.4 eV. The hybridization strength V is related to the gap Δ by $\Delta=2V^2/B$, where B is the bandwidth of the related conduction band. The solution for the spectrum is equivalent to the solution for the bremsstrahlung isochromat spectroscopy spectrum in cerium material, replacing the electrons by holes and inserting the form for the valence bands obtained from the band-structure calculations. The electronic gaps in the photoemission spectra are given for the interaction with parabola (P_1) as $\Delta_1 \sim 80$ meV observed in panel (A) in Fig. 8 and for the interaction with parabola (P_2) as $\Delta_2 \sim 45$ meV observed in the panels (C) and (D) in Fig. 8. In order to reproduce the spectrum, we vary ϵ_f, the eightfold degenerate f level.

The spectrum (open symbols in panel (B) in Fig. 8) is obtained by integrating the angle-resolved photoemission data between 0° and 20° at 21.2 eV and subtracting the contribution from the Rh $4d$ band using a Doniach-Sunjic line shape.[32] Furthermore, we subtracted the intensity from the $4f_{5/2}$ surface state centered at 2 eV using a Lorentzian and a uniform background as in Ref. 24. The subtraction is rather tedious and perfect agreement with the calculation cannot be expected. The features of interest are two strong intensity regions, one centered at −1.35 eV and the other at −45 meV with intensity ratio of 2:3. The peak at −1.35 eV which mimics the $4f_{5/2}$ excitation is approximated by a Lorentzian with linewidth of ∼55 meV where we subtracted the background. As noted earlier, the feature at −0.7 eV is due to a surface state. Its emission is approximated by a Lorentzian with linewidth of ∼230 meV (see the dashed line). The feature at higher binding energy is slightly asymmetric, and some additional intensity around −1.1 eV could not be removed properly.[33]

The result of the GS simulation is shown as a solid line in panel (B) in Fig. 8. The simulation yields an energy $\epsilon_f \approx -1.4$ eV and a hole concentration of 0.99 in the $4f^{14}$ shell, i.e., the full Yb^{3+} moment. The asymmetry of the peak at 50 meV can be explained by the arguments of Doniach and Sunjic.[32]

In the spin-fluctuation limit with the f-level occupancy very close to 1, an estimate for the Kondo temperature can be obtained in the GS scheme[25] as

$$T_K \equiv \frac{\delta}{k_B} = \frac{|\epsilon_f| - \Delta E}{k_B} \approx 30 \text{ K}, \tag{1}$$

where k_B is the Boltzmann constant. The energy gain through the hybridization is given as

$$\Delta E = N_f \left(\sum_i \int \frac{|V_i(\epsilon)|^2}{\Delta E - \epsilon_f - \epsilon} d\epsilon \right). \tag{2}$$

The hybridization is determined as $|V_i(\epsilon)|^2 = \Delta_i \sqrt{B_i^2 - \epsilon^2}/B_i$. Kondo temperatures obtained with this method yield only an approximate Kondo scale. However, a Kondo temperature of a few tens of Kelvin is corroborated by the results from macroscopic experiments which yielded $T_K \approx 24$ K.[9,10]

Previous band-structure calculations[15,28] resulted in the $4f^{14}$ ground state for the Yb ion. This leads to $4f_{7/2}$ electronic states at 100–200 meV and $4f_{5/2}$ states at 1.3 eV below E_F.[15,34] Taken literally, one is tempted to say that this provides an alternative interpretation for the $4f$ peaks at E_F and at −1.3 eV. With this background, the origin of a peak at 1.3 eV needs further clarification. We also recall that the GS scheme considers the emission from a mixture of $4f^{13}$ and $4f^{14}$ orbitals and neglects the true many-body essence of the Kondo resonance. With this in mind, the interpretation of the $4f$ peaks near E_F and 1.3 eV is not straightforward anymore and raises severe doubts if an analysis according the GS

scheme is justified. The interpretation of these two peaks is likely to be given, in an atomistic framework, by Gerken[29] and which has been used for SmB_6 and sometimes also for Yb-related material.[35,36] In this case, the valency is reduced to approximately +2.9,[22] which, however, interferes with macroscopic experiments.[9] Given the serious deficiency of recent band-structure calculations in getting the correct experimental picture for the Yb $4f^{13}$ ion, which is then progressively screened at low temperature due to the Kondo effect, and given our GS-scheme simulation which provides a reasonable electronic spectrum and T_K, in balance, we favor the Kondo resonance interpretation. We expect time-dependent two-photon photoemission spectroscopy and DMFT calculations on pure Yb to yield more information on the nature of these peaks.

We address the recent claim of $YbRh_2Si_2$ being a mixed valent.[15,22] If a d band crosses the f spectrum and the Fermi energy overlaps the f configurational levels to within the hybridization energy, we have a mixed valence compound, i.e., the Yb ions occur both as Yb^{3+} with electronic $4f^{13}$ configuration or Yb^{2+} with $4f^{14}$ configuration. Panels (C) and (D) in Fig. 8, however, display that the hybridization energy is smaller than the distance to the Fermi level, i.e., 50 meV, and hence the valency is close to +3.

D. Constant energy cuts at 21.2 eV

The results of our band-structure calculations suggest that the FS of $LuRh_2Si_2$ does not deviate significantly from the one of $YbRh_2Si_2$, plotted in Fig. 4.

The lower panel in Fig. 9 shows a FS map of $LuRh_2Si_2$ obtained at a photon energy of 21.2 eV. We integrated the intensity over an energy window of 2 meV at E_F. This integration window is extremely narrow. It is imposed by the comparison to the FS of $YbRh_2Si_2$ where the intensity of the $4f_{7/2}$ excitations appears close to the Fermi level and might falsify the intensity pattern. We distinguish clearly three different regions. Right in the center of the BZ, we observe a bright intensity $\mathcal{J}'$ which, according Sec. IV B, is the inner part of the complex jungle-gym sheet forming a tiplike structure. $\mathcal{D}$ is a cut through the donutlike FS sheet centered around the Z point of the BZ. Its intensity is blurred out because of considerable k_z dispersion. $\mathcal{J}$ is again a cut through the complex jungle-gym sheet at the border of the BZ. For a better understanding, compare to Fig. 4.

The upper panel in Fig. 9 shows a FS map of $YbRh_2Si_2$ obtained at the same photon energy of 21.2 eV. We again integrated the intensity over an energy window of 2 meV centered at the Fermi level determined on the gold reference sample. In accordance with the LDA+U+SOC calculations, the FS splits again into three different parts. At $\tilde{\Gamma}$, there is a small tiplike area $\mathcal{J}'$ with a high intensity. At the boundary of the BZ, the very distinct arms of the FS sheet $\mathcal{J}$ show strong intensities. As indicated by the cut along $\tilde{\Gamma}\tilde{X}$ in Fig. 7, it appears that for some particular crystal momenta the sheet $\mathcal{J}$ splits into two parts which have been labeled (d_1) and (d_2), respectively. An momentum distribution curve and/or EDC analysis reveals that these excitations have a relatively light effective mass of $m_{eff} \approx 1.2 m_e$. The intensity pattern labeled $\mathcal{D}$ shows a cut through the FS displaying Rh $4d$ and Yb $5d$ characters and forming the same donut-shaped sheet as observed in $LuRh_2Si_2$.

We observe that at least qualitatively, the Fermi surfaces of $LuRh_2Si_2$ and $YbRh_2Si_2$ agree. This confirms the results of the band-structure investigations which obtained nearly identical FS for both materials. Hence, we conclude that the Yb $4f$ electron contribution to actively form the FS is small at 14 K.

V. CONCLUSIONS

In this paper, we have presented the results of an electronic band-structure calculation within a relativistic framework including correlation corrections for $YbRh_2Si_2$. The characteristic of the electronic structure is the $4f^{13}$ ground state as required by the Curie-Weiss moment that is observed at high temperature. A small FS cylinder of $4d_{x^2-y^2}$ symmetry is centered at Γ, a fluted donut $\mathcal{D}$ surface situated around the upper zone face midpoint Z, and a multiply connected jungle-gym $\mathcal{J}$ surface. The angle-resolved photoemission spectrum manifests (true many-body) intensities originating from $4f^{13}_{7/2}$ and $4f^{13}_{5/2}$ final-state excitations separated by 1.3 eV, the value for the spin-orbit interaction obtained from the calculation. These excitations are eightfold (sixfold) degenerate and do not manifest the splitting due to the anisotropic Coulomb interaction inherent to the single-particle energy states.

An analysis of the $4f$ spectrum $\rho_\nu(\epsilon)$ according the degenerate Anderson impurity model using the parameters obtained from the band-structure calculations explains the appearance of a peak related to the $4f_{7/2}$ excitations at 45 meV below E_F. The Kondo splittings obtained from the band-structure calculations can be compared to the electronic gaps in the photoemission spectra. In a GS framework, the splittings are $V(\epsilon_F)=V/\pi \approx 33$ meV at Γ and ≈ 16 meV at the BZ boundaries. These values agree with those obtained from the LDA+U+SOC calculation. The Kondo temperature $T_K \sim 30$ K and full Yb^{3+} moment are in agreement with the results from macroscopic experiments.

The band structure and FS of $LuRh_2Si_2$ and $YbRh_2Si_2$ are compared. The absence of very flat bands in the Lu compound provides confirmation for the $4f$ nature of these bands in the Yb compound. Both compounds show very similar Fermi-surface features. At the center of the BZ, we cut a tiplike sheet which is part of the jungle-gym FS J. The same sheet is visible with high intensity embracing the X point of the BZ. Additionally, at 21.2 eV, we observe a large surface centered at the Z point of the BZ in the form of a donut. There is no clear difference between the FS of both materials observed, neither theoretically nor experimentally. This indicates that the spectral weight of the $4f$ bands do not contribute significantly in forming the FS at 14 K.

ACKNOWLEDGMENTS

This work has benefited from partial financial support of the Schweizerische Nationalfonds zur Förderung der wissenschaftlichen Forschung, the US-DOE Grant No. DE-FG03-

01ER45876, and Grant No. NSF-DMR 0433560. W.E.P. acknowledges support and stimulating atmosphere of the Department of Energy's Stewardship Science Academic Alliances Program, and the hospitality of the Alexander von Humboldt Foundation during the later stages of this work. W.E.P. and Z.P.Y. acknowledge important interactions within DOE's Computational Materials Science Network team studying strongly correlated materials.

[1] G. R. Stewart, Rev. Mod. Phys. **73**, 797 (2001).
[2] B. Bogenberger and H. v. Lohneysen, Phys. Rev. Lett. **74**, 1016 (1995).
[3] F. M. Grosche, S. R. Julian, N. D. Mathur, and G. G. Lonzarich, Physica B **223-224**, 50 (1996).
[4] I. R. Walker, F. M. Grosche, D. M. Freye, and G. G. Lonzarich, Physica C **282-287**, 303 (1997).
[5] P. Estrella, A. de Visser, F. R. de Boer, G. J. Nieuwenhuys, L. C. J. Pereira, and M. Almeida, Physica B **259-261**, 409 (1999).
[6] J. Kondo, Prog. Theor. Phys. **32**, 37 (1964).
[7] M. A. Ruderman and C. Kittel, Phys. Rev. **96**, 99 (1954).
[8] K. Ishida, D. E. MacLaughlin, O. O. Bernal, R. H. Heffner, G. J. Nieuwenhuys, O. Trovarelli, C. Geibel, and F. Steglich, Physica B **326**, 403 (2003).
[9] O. Trovarelli, C. Geibel, S. Mederle, C. Langhammer, F. M. Grosche, P. Gegenwart, M. Lang, G. Sparn, and F. Steglich, Phys. Rev. Lett. **85**, 626 (2000).
[10] P. Gegenwart, J. Custers, C. Geibel, K. Neumaier, T. Tayama, K. Tenya, O. Trovarelli, and F. Steglich, Phys. Rev. Lett. **89**, 056402 (2002).
[11] O. Trovarelli, J. Custers, P. Gegenwart, C. Geibel, P. Hinze, S. Mederle, G. Sparn, and F. Steglich, Physica B **312-313**, 401 (2002).
[12] J. Custers, P. Gegenwart, H. Wilhelm, K. Neumaler, Y. Tokiwa, O. Trovarelli, C. Geibel, F. Steglich, C. Pépin, and P. Coleman, Nature (London) **424**, 524 (2003).
[13] K. Ishida, K. Okamoto, Y. Kawasaki, Y. Kitaoka, O. Trovarelli, C. Geibel, and F. Steglich, Phys. Rev. Lett. **89**, 107202 (2002).
[14] S. Paschen, T. Luhmann, S. Wirth, P. Gegenwart, O. Trovarelli, C. Geibel, F. Steglich, P. Coleman, and Q. Si, Nature (London) **432**, 881 (2004).
[15] M. R. Norman, Phys. Rev. B **71**, 220405(R) (2005).
[16] Q. Si, S. Rabello, K. Ingersent, and J. L. Smith, Phys. Rev. B **68**, 115103 (2003).
[17] S. Hüfner, *Photoelectron Spectroscopy* (Springer Verlag, Berlin, 1995).
[18] P. W. Anderson, Phys. Rev. **124**, 41 (1961).
[19] K. Schwarz, P. Blaha, and G. K. H. Madsen, Comput. Phys. Commun. **147**, 71 (2002).
[20] J. P. Perdew, K. Burke, and M. Ernzerhof, Phys. Rev. Lett. **77**, 3865 (1996).
[21] M. D. Johannes and W. E. Pickett, Phys. Rev. B **72**, 195116 (2005).
[22] S. Danzenbacher, Y. Kucherenko, D. V. Vyalikh, M. Holder, C. Laubschat, A. N. Yaresko, C. Krellner, Z. Hossain, C. Geibel, X. J. Zhou, W. L. Yang, N. Mannella, Z. Hussain, Z.-X. Shen, M. Shi, L. Patthey, and S. L. Molodtsov, Phys. Rev. B **75**, 045109 (2007).
[23] For other examples, consider K. Takegahara and Y. Kaneta, J. Phys. Soc. Jpn. **60**, 4009 (1991); I. I. Mazin and S. L. Molodtsov, Phys. Rev. B **72**, 172504 (2005).
[24] F. Patthey, J.-M. Imer, W.-D. Schneider, H. Beck, Y. Baer, and B. Delley, Phys. Rev. B **42**, 8864 (1990).
[25] O. Gunnarsson and K. Schönhammer, Phys. Rev. B **28**, 4315 (1983).
[26] J. W. Allen, S.-J. Oh, I. Lindau, J. M. Lawrence, L. I. Johansson, and S. B. Hagström, Phys. Rev. Lett. **46**, 1100 (1981); J. W. Allen, G. H. Gweon, H. T. Schek, L. Z. Liu, L. H. Tjeng, J. H. Park, W. P. Wllis, C. T. Chen, O. Gunnarsson, O. Jepsen, O. K. Andersen, and Y. Dalichaouch, J. Appl. Phys. **87**, 6088 (2000).
[27] S. Suga, A. Sekiyama, S. Imada, A. Shigemoto, A. Yamasaki, M. Tsunekawa, C. Dallera, L. Braicovich, T.-L. Lee, O. Sakai, T. Ebihara, and Y. Onuki, J. Phys. Soc. Jpn. **74**, 2880 (2005).
[28] S. Danzenbächer, Y. Kucherenko, C. Laubschat, D. V. Vyalikh, Z. Hossain, C. Geibel, X. J. Zhou, W. L. Yang, N. Mannella, Z. Hussain, Z.-X. Shen, and S. L. Molodtsov, Phys. Rev. Lett. **96**, 106402 (2006).
[29] F. Gerken, J. Phys. F: Met. Phys. **13**, 703 (1983).
[30] L. H. Tjeng, S.-J. Oh, E.-J. Cho, H.-J. Lin, C. T. Chen, G.-H. Gweon, J.-H. Park, J. W. Allen, T. Suzuki, M. S. Makivić, and D. L. Cox, Phys. Rev. Lett. **71**, 1419 (1993).
[31] A. Sekiyama, T. Iwasaki, K. Matsuda, Y. Saitoh, Y. Onuki, and S. Suga, Nature (London) **403**, 396 (2000).
[32] S. Doniach and M. Sunjic, J. Phys. C **3**, 285 (1970).
[33] F. D. M. Haldane, Phys. Rev. Lett. **40**, 416 (1978); J. H. Jefferson, J. Phys.: Condens. Matter **10**, 3589 (1997).
[34] G. Knebel, R. Boursier, E. Hassinger, G. Lapertot, P. G. Noklowitz, A. Pourret, B. Salce, J. P. Sanchez, I. Sheikin, P. Bonville, H. Harima, and J. Flouquet, J. Phys. Soc. Jpn. **75**, 114709 (2006).
[35] V. N. Antonov, B. N. Harmon, and A. N. Yaresko, Phys. Rev. B **66**, 165209 (2002).
[36] R. I. R. Blyth, J. J. Joyce, A. J. Arko, P. C. Canfield, A. B. Andrews, Z. Fisk, J. D. Thompson, and R. J. Bartlett, P. Riseborough, J. Tang, and J. M. Lawrence, Phys. Rev. B **48**, 9497 (1993).